International Journal of Industrial Electronics, Control and Optimization © 2021 IECO
Vol. 4, No. 2, pp. 257-266, April (2021)

An Improved Sliding Mode Controller for DC/DC Boost Converters Used in EV Battery Chargers with Robustness against the Input Voltage Variations

Gholamreza Mohebalizadeh [1], Hasan Alipour [†,2], Leila Mohammadian[3], Mehran Sabahi[4]

[1, 2, 3] Department of Electrical Engineering, Islamic Azad University, Shabestar Branch, Shabestar, Iran.
[4] Department of Electrical and Computer Engineering, University of Tabriz, Tabriz, Iran.

ABSTRACT

An Electric Vehicle Battery Charger (EVBC) faces serious challenges such as continuous charging voltage ripple, charging speed, input voltage level variations, and its ability to adapt to the Battery State of Charge (BSOC). A proper controller has an important role to play in preparing for all mentioned above. A nonlinear controller such as a Sliding Mode Controller (SMC) is eminently suitable for solving these problems. Therefore, this work presents an improved SMC for taking the control of a DC/DC boost converter such as an EVBC. The proposed controller has a more robust structure when exposed to significant variations of input voltage than the other SMCs. Therefore, this allows the application of various power supplies as input voltages in EVBC stations. The EVBC power and battery voltage/capacity in this converter are assumed to be 14 kW and 400V/60Ah, respectively. The simulation results in Matlab Simulink verify the controller's high performance compared with other SMCs.

Article Info

Keywords:
Battery State of Charge (BSOC), Electric Vehicle Battery Charger (EVBC), Mean Displacement Error (MDE), Renewable Energy Source (RES), Sliding Mode Controller (SMC)

Article History:
Received 2020-05-31
Accepted 2020-11-09

I. INTRODUCTION

An increase in oil prices and concerns over air pollution are prompting the introduction of electric vehicles (EVs) and plug-in hybrid EVs (PHEVs). Nowadays and in the immediate future, considerable regards to establishing stations fully equipped with EVBC are required. On-board and off-board are two classifications of EVBC [1]. On-board EVBCs are installed in EVs. Therefore, their application is faced with main constraints such as weight, volume, and power limitations. Off-board EVBCs, which do not have those constraints, are installed in EVBC stations [2]. Moreover, these EVBCs can be supplied by 3-phase electric grid, ancillary batteries, and Renewable Energy Sources (RESs) such as Photovoltaic Cells (PVCs) and wind turbines [3]. Therefore, a perfect match must occur with these input power supplies. Moreover, the charging current and voltage should be in accordance with the BSOC [4].

These can be fully implemented by applying an SMC. SMCs face serious challenges such as eminently suitable designation of sliding surface and state reference values [5-7]. The output voltage level of EVBC gradually varies in accordance with the SOC. Therefore, the input current also varies and a proper consideration of input reference current requires a considerable degree of flexibility for the controller [8]. Because of using fuel cells as the input voltage and limitation of voltage gain of the boost converter, it is possible to reach the reference voltage level (400V) by considering a large number of cells. So, this consideration increases the number of fuel cells. The constant input voltage and reference

[†] Corresponding Author: hasan.alipour2006@gmail.com
Tel: +98-9141090533, Department of Electrical Engineering, Islamic Azad University, Shabestar Branch, Shabestar, Iran.

current's assumption are the defects of this controller.

In [9], the sliding mode controller for a single-switch cascade converter is proposed. The constant input reference current assumption is the main defect of this controller. In [10], a 3-stage controller with a Dual Active Bridge (DAB) is proposed. The first stage has the Power Factor Correction (PFC) function, and the controller strategy is based on the status of DC link voltage proportional with the instantaneous SOC. Therefore, the controller is complicated and cannot be used in the other input power supplies. In [11], an on-board EVBC is proposed with a compensator consisting of zeta and boost converters cascaded with the Cuk converter. The compensator is used to decrease current and voltage ripples to descend the filter capacitor size resulting in the complication of the controller. In [12], a non-PWM sliding mode controller for a Sheppard-Taylor converter in presented. The reference current proportional with the voltage error is considered. Because of using the non-PWM sliding mode controller, the switching frequency is variable. A cascade buck and boost are applied in [13] in which different duty cycles with variable phase shift structures are considered. The efficiency and power factor are increased. Moreover, the total harmonic distortion is decreased, but the control system is highly complex. A current control in a buck DC/DC converter by means of a PWM-based sliding mode technique is presented in [14]. The output voltage/input current errors as state variables are applied in sliding surface consideration in this work. Moreover, the input reference current is considered a constant quantity. Therefore, the negative effect of input voltage variations in the converter cannot be controlled. A multi-input EVBC using SMC is presented in [15]. The converter's structure is well designed, but the applied state variables in the sliding surface are considered unsuitable and insufficient. More state variables should be applied in complex structures such as these certain types of converters.

This paper proposes an improved SMC to control a DC/DC boost converter as an EVBC. The integral function of the charging voltage error is considered as the input reference current. Therefore, a more robust structure in the input power supply voltage variations is made by this controller, and this distinctive characteristic allows flexibility in the input voltage level variations. Moreover, a minimal amount of charging voltage error, ripple, and mean displacement percentage can be attained in the proposed controller compared to the other SMCs.

This paper consists of seven sections. In section II, a DC/DC boost converter as an EV battery charger is introduced. Section III reviews common sliding mode control approaches. Section IV introduces the proposed controller. In section V, the proposed PWM sliding mode controller simulation results in MATLAB Simulink environment are presented and compared with the other SMCs. Finally, Section VI presents the concluding points.

II. DC/DC BOOST CONVERTER AS AN EVBC

A general battery charger is designed and constructed by a DC/DC converter in a simple structure. The DC input voltage can be prepared by different kinds of RESs. An AC/DC converter is required to supply the grid-line/wind turbine power to its input. The possible variations in these AC powers may cause trouble in the battery charger.

Hint1:

General battery chargers have a fixed-level input voltage related to their application, but an EVBC can be supplied by some different types of input power supplies in an EVBC station. Therefore, an EVBC with robustness against input voltage variations can also be used as a general battery charger.

Hint2:

An AC/DC converter is required in an EVBC station whenever a one-(or three-)phase grid power or a wind turbine is used. Moreover, the input DC voltage variation ranges of EVBC are considered about ten volts in the proposed controller. It is important to mention that the input voltage variation is a cause for the variation of wind/line power. A multi-input DC/DC converter is also required whenever the PV cells are applied to use ancillary batteries beside those cells. The output voltage variation that is applied as an input of the EVBC will be low enough whenever this multi-input converter is well designed.

Fig. 1 shows the DC/DC boost EV battery charger's structure with its controller. The voltage and current gain and the duty cycle equations are presented as (1).

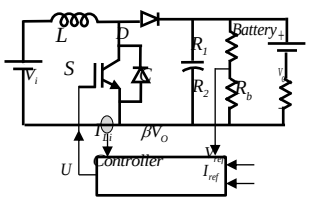


Fig.1. A schematic diagram of the DC/DC Boost Converter

$$D = \frac{T_{on}}{T_S}; G_V = \frac{V_o}{V_i} = \frac{1}{1-D}; G_I = \frac{I_b}{I_L} = 1 - D; \quad (1)$$

where D, V_o, V_i, I_b, I_L, G_I, G_v, T_{on}, and T_s are the duty cycle, the output and input voltage, the output and input current, the current and voltage gain, the ON time of the IGBT function duration, and the switching period, respectively. The output

voltage is instantaneously compared with the reference voltage. The IGBT gate gets no pulses when the output voltage reaches the reference voltage. By applying the equation of Kirchhoff's law, the main boost converter's equation is obtained as (2).

$$\left\{\begin{matrix} V_L = V_i - V_o \times (1-D) \\ i_c = i_L \times (1-D) - i_b \end{matrix}\right\} \Rightarrow \left\{\begin{matrix} \frac{di_L}{dt} = \frac{v_i}{L} - \frac{v_o}{L} \times \bar{D} \\ \frac{dv_o}{dt} = \frac{i_L}{C} \times \bar{D} - \frac{v_o}{R_L C} \end{matrix}\right\} \quad (\bar{D} = 1 - D) \tag{2}$$

where L, C, i_C, and R_L are inductance, capacitance, the capacitor's current, and the output resistance, respectively.

III. Common SMC Approaches

A. Mathematical Formulation

Consider a nonlinear time-dependent switching system defined by the following equation [18]:

$$\dot{x}(t) = g(x(t)) + \Phi(x(t)).u(t)$$

where $x(t)$ is the state variable vector in an n-dimensional space R_n, $g(0)$ and $\phi(0)$ are the smooth vector fields in the same space, and $u(t)$ is the discontinuous control action expressed as:

$$u(t) = \begin{Bmatrix} U^+ \ldots if, S(x,t) > 0 \\ U^- \ldots if, S(x,t) < 0 \end{Bmatrix} \tag{3}$$

where U^+ and U^- are either scalar values or scalar functions of $x(t)$ and $S(x, t)$ is the instantaneous feedback-tracking trajectory of the system and is a predetermined function of the state variables. Typically, for the ease of design and implementation, $S(x, t)$ is chosen as a linear combination of the weighted values of the state variables and is given as

$$S(x,t) = \sum_{i=1}^{m} \alpha_i x_i(t) \tag{4}$$

where α_i for i = 1 to m denotes the set of the control parameters known as sliding coefficients and $x_i(t) \in x(t)$. A system with this description is said to exhibit SM property when all the required conditions, namely hitting, existence, and stability conditions, are met.

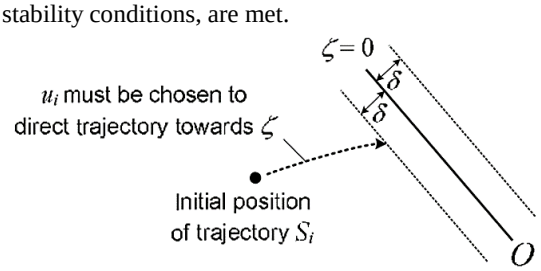


Fig.2. Trajectory S converging to the sliding manifold in the SM control process when the hitting condition is fulfilled.

1) Hitting Condition

The objective of the hitting condition is to ensure that regardless of the location of the initial condition, the corresponding control decision will direct the trajectory of the system to approach and eventually reach, within a vicinity of δ, the sliding manifold (see Fig. 2). Assume that the system is at an initial state with vector $x_i=x(t=0)$ and a trajectory $S_i=S(t=0)$, which is located at a distance away from the sliding manifold ζ = 0. The necessary and sufficient condition for the system to satisfy the hitting condition is that the resulting controls $u_i=u(t>0)$ produces a state-variable vector $x(t>0)$ and consequently a controlled trajectory $S(t>0)$, which satisfies the following inequality:

$$S \frac{dS}{dt} < 0 \ldots for \; S \neq 0 \quad and \quad \lim_{S \to 0} S \frac{dS}{dt} \geq 0 \tag{5}$$

The inequality (5) is a partial result of the Lyapunov second theorem on stability, of which the Lyapunov function candidate is

$$V(s) = \frac{1}{2} S^2 \tag{6}$$

The compliance of (5) signifies that at a position not within the vicinity of the sliding manifold, the state trajectory S is continuously being attracted and is always converging to the sliding manifold ζ = 0 for t > 0, and that the choice of $u_i = u(t) > 0$ is supporting this attraction. Hence, one important and fundamental aspect of designing an SM control is to first determine, for a desired set of control parameters (sliding coefficients), the suitable discontinuous control action for the system, as described in (3). In other words, the design of U^+ and U^- would have to ensure that the hitting condition is always satisfied for a given system.

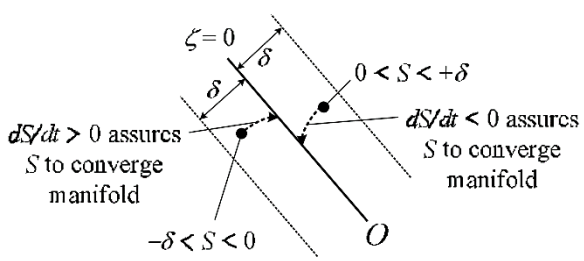


Fig. 3. Trajectory S at a location within the vicinity of sliding manifold $0 < |S| < \delta$ converging to the sliding manifold in SM control process when the existence condition is fulfilled.

2) Existence Condition

Having the system already designed to fulfil the hitting condition, it is then necessary to check if the system also

complies with the existence condition, which ensures that once the trajectory is at locations within the vicinity of the sliding manifold such that $0 < |S| < \delta$, it is still always directed toward the sliding manifold, as illustrated in Fig. 3. The existence condition of the SM operation can be determined by inspecting only the local reachability condition of $S.dS/dt<0$ such that in the domain of $0 < |S| < \delta$, the condition

$$\lim_{S \to 0} S.\frac{dS}{dt} < 0 \tag{7}$$

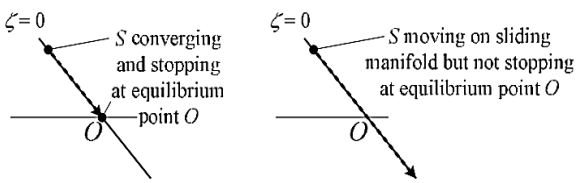
must be satisfied. This can be expressed as:

$$\left\{ \lim_{S \to 0^-} S.\frac{dS}{dt} < 0 \right\} ; \left\{ \lim_{S \to 0^+} S.\frac{dS}{dt} \right\} \tag{8}$$

In a physical sense, the existence condition can be understood as being a requirement for the controlled trajectory and its time derivative to have opposite signs in the vicinity of a discontinuous surface

3) Stability Condition

In addition to the existence condition, the control action and sliding coefficients must be designed to comply with the stability condition. This is to ensure that in the event of operating in the sliding phase, the desired sliding manifold will always direct the trajectory toward a stable equilibrium point. Failure to achieve this will lead to an unstable SM system. Fig. 4(a) shows the trajectory of a system under SM operation stabilizing at the desired point of equilibrium O when stability condition is fulfilled, and Fig. 4(b) shows the same trajectory moving pass O when stability condition is not fulfilled.



(a) Stable (b) Unstable

Fig.4. Trajectory S moving on the sliding manifold and (a) converging to the desired point of equilibrium O when stability condition is fulfilled, and (b) passing through and not stopping at the desired point of equilibrium O when stability condition is not fulfilled.

In general, the stability of a system is obtained by ensuring that the eigenvalues of the Jacobian of the system at the steady-state region have negative real parts. In the following, we will consider how the stability condition of the SM operation can be found for a system with a linear sliding manifold and a system with a nonlinear sliding manifold.

To define the problem and determine the objectives of the proposed method, it is required to explain some conventional sliding mode controllers used in EV battery chargers.

B. Sliding mode voltage control (SMVC)

This control method only considers the output voltage as a reference, which is more suitable for the buck converters [16]. The sliding surface and the converter's duty cycle as the control input are presented as (9) and (10), respectively.

$$\begin{aligned} S &= a_1 X_1 + a_2 X_2 + a_3 X_3 \\ &= a_1(V_{ref} - \beta V_o) + a_2(-\frac{\beta}{C} i_C) + a_3 \int (V_{ref} - \beta V_o) dt \end{aligned} \tag{9}$$

where S, X_n, α_n (n = 1, 2, 3), V_{ref}, and β are the sliding surface, the state and coefficient variables, the reference voltage, and the output voltage sampling percent, respectively. The controller's output equation as the switch's duty cycle is obtained as (10).

$$U_{eq} = \frac{-K_{p_1} i_C + \beta(V_o - V_i) + K_{p_2}(V_{ref} - \beta V_o)}{\beta(V_o - V_i)} \tag{10}$$

where Kp_1 and Kp_2 are calculated according to [17].

C. Indirect Sliding Mode Current Control (ISMC)

In this method, the output voltage and the input current references are simultaneously considered. The input current reference is considered in form of a coefficient of the output voltage error [18]. The sliding surface and the duty cycle equations are presented as (11) and (12), respectively.

$$\begin{aligned} S &= a_1 X_1 + a_2 X_2 + a_3 X_3 \\ &= a_1 i_{Lref} - a_1 i_L + a_2(V_{ref} - \beta V_o) \\ &+ a_3 \int \left[(1+K)(V_{ref} - \beta V_o) - i_L \right] dt \\ &\Rightarrow i_{Lref} = K(V_{ref} - \beta V_o) \end{aligned} \tag{11}$$

where X_1, X_2, X_3, and i_{Lref} are the current/voltage error, the integral summation of the voltage, and current errors, respectively. The input reference current is a proportion of the output voltage error. Moreover, the coefficient K is considered sufficiently large.

$$U_{eq} = \frac{-\beta(V_i - V_o) + \beta K_2 i_C + \beta K_1(V_{ref} - \beta V_o) - \beta K_3 i_L}{\beta V_o} \tag{12}$$

The calculation steps of the coefficients K_1, K_2, and K_3 are

given in [17].

D. Double Integral Sliding Mode Control (DISMC)

By considering an additional integral variable at the sliding surface, the ISMC controller's steady-state error is improved in this strategy. The sliding surface and the duty cycle equations are presented as (13) and (14), respectively [17].

$$S = a_1\left[K(V_{ref} - \beta V_o) - i_L\right] + a_2(V_{ref} - \beta V_o) + a_3\int\left[K(V_{ref} - \beta V_o) - i_L + V_{ref} - \beta V_o\right]dt + a_4\iint\left[K(V_{ref} - \beta V_o) - i_L + V_{ref} - \beta V_o\right]dtdt \quad (13)$$

$$U_{eq} = \frac{(1 + K_1 / R_L)V_o - V_i + KK_2(V_{ref} - \beta V_o) - (K_1 + K_2)i_L + KK_3\int(V_{ref} - \beta V_o)dt - K_3\int i_L dt}{V_o - K_1 i_L}$$

$$K_1 = \frac{L\beta}{C}(K + \frac{a_2}{a_1}); K_2 = L\frac{a_3}{a_1}; K_3 = L\frac{a_4}{a_1} \quad (14)$$

where K_n (n = 1, 2, 3) is calculated according to the steps presented in [18].

IV. Proposed Integral SMC (PISMC)

In the proposed method, the reference current is considered proportional to the integral of the output voltage error. The sliding surface variables in the proposed controller are considered as (15).

$$\begin{aligned} X_1 &= i_{ref} - i_L; i_{ref} = K\int(V_{ref} - \beta V_o)dt \\ X_2 &= V_{ref} - \beta V_o \\ X_3 &= \int X_1 dt \end{aligned} \quad (15)$$

The sliding surface is presented as (16).

$$\begin{aligned} S &= a_1X_1 + a_2X_2 + a_3X_3 \\ S &= a_1(K\int(V_{ref} - \beta V_o)dt - i_L) + \\ &a_2(V_{ref} - \beta V_o) + a_3\int(K\int(V_{ref} - \beta V_o)dt - i_L)dt \end{aligned} \quad (16)$$

The 4th part of the sliding surface used in the DISMC method is not necessary. Moreover, the sliding surface must reach zero (or close to zero) at infinity to maintain asymptotic stability so as (17):

$$\dot{S} = a_1K(V_{ref} - \beta V_o) - a_1\frac{di_L}{dt} - a_2\beta\frac{dV_o}{dt} + a_3K\int(V_{ref} - \beta V_o)dt - a_3i_L = 0 \quad (17)$$

As: $V_L = L\frac{di_L}{dt}; V_L = V_i - V_o(1 - U_{eq})$ So:

$$a_1K(V_{ref} - \beta V_o) - \frac{a_1}{L}\left[V_i - V_o(1 - U_{eq})\right] - \frac{a_2\beta}{C}i_c + a_3K\int(V_{ref} - \beta V_o)dt - a_3i_L = 0 \quad (18)$$

By putting the ic and according to (19), (20) is attained.

$$i_C = (1 - U_{eq})i_L - \frac{V_o}{R_L} \quad (19)$$

$$a_1K(V_{ref} - \beta V_o) - \frac{a_1}{L}\left[V_i - V_o(1 - U_{eq})\right] - \frac{a_2\beta}{C}\left[(1 - U_{eq})i_L - \frac{V_o}{R_L}\right] + a_3K\int(V_{ref} - \beta V_o)dt - a_3i_L = 0 \quad (20)$$

where R_L is the internal battery resistance and varies with the battery temperature. By multiplying (20) in L/α_1, (21) is attained.

$$LK(V_{ref} - \beta V_o) - V_i + V_o - V_oU_{eq} - \frac{La_2\beta}{Ca_1}i_L + \frac{La_2\beta}{Ca_1}U_{eq}i_L + \frac{La_2\beta}{Ca_1} \times \frac{V_o}{r_L} + \frac{La_3K}{a_1}\int(V_{ref} - \beta V_o)dt - \frac{La_3}{a_1}i_L = 0 \quad (21)$$

By simplification of (21), (22) is attained.

$$\begin{aligned} &LK(V_{ref} - \beta V_o) - V_i + V_o - K_1i_L - K_2i_L + K_1\frac{V_o}{r_L} + \\ &+K_2K\int(V_{ref} - \beta V_o)dt = U_{eq}(V_o - K_1i_L) \\ &K_1 = \frac{La_2\beta}{Ca_1}; K_2 = \frac{La_3}{a_1} \end{aligned} \quad (22)$$

Finally, the main controller's output as the duty cycle is obtained as (23)

$$U_{eq} = 1 - \frac{-K_1\frac{V_o}{R_L} - LK(V_{ref} - \beta V_o) + V_i + K_2i_L - K_2K\int(V_{ref} - \beta V_o)dt}{V_o - K_1i_L} \quad (23)$$

The coefficients α_n (n = 1, 2, 3), K, and K_n (n = 1, 2) are unknown in (23). The system's stability condition is guaranteed (the positioning of the system's poles on the left side of the imaginary axis) [18].

In the boost converter as Eq. (2):

$$\left\{\begin{array}{l} \frac{di_L}{dt} = \frac{v_i}{L} - \frac{v_o}{L}\frac{-K_1\frac{V_o}{R_L} - LK(V_{ref} - \beta V_o) + V_i + K_2i_L - K_2K\int(V_{ref} - \beta V_o)dt}{V_o - K_1i_L} \\ \frac{dv_o}{dt} = \frac{i_L}{C}\frac{-K_1\frac{V_o}{R_L} - LK(V_{ref} - \beta V_o) + V_i + K_2i_L - K_2K\int(V_{ref} - \beta V_o)dt}{V_o - K_1i_L} - \frac{v_o}{R_LC} \end{array}\right\} \quad (24)$$

Given the nonlinearity (23), the Laplace method cannot be used to solve it. Using the small-signal method for variables around the point of equilibrium in small variations is considered. By applying the energy conservation law around the equilibrium point as (25), (26) is attained

$$I_L = \frac{V_o^2}{V_iR_L}; \quad y \quad = oV \tilde{} + \tilde{v}_o; v_L \quad i \quad _L = \tilde{} \quad I_L; + i \quad i \quad ; v \quad i \quad = \quad r \quad e \quad f \quad V \quad \beta \quad \quad (25)$$

$$I_{ref} = I_L; K \gg 1; V_o \gg \tilde{v}_o; I_L \gg \tilde{i}_L$$

$$\begin{cases} \dfrac{d(I_L+\tilde{i}_L)}{dt}=\dfrac{v_i}{L}-(\dfrac{V_o+\tilde{v}_o}{L})* \\ \dfrac{-K_1\dfrac{(V_o+\tilde{v}_o)}{R_L}-LK\left[V_{ref}-\beta(V_o+\tilde{v}_o)\right]+V_i+K_2(I_L+\tilde{i}_L)-K_2K\int\left[V_{ref}-\beta(V_o+\tilde{v}_o)\right]dt}{V_o-K_1\dfrac{V_o^2}{V_iR_L}} \\ \dfrac{d(V_o+\tilde{v}_o)}{dt}=\dfrac{(I_L+\tilde{i}_L)}{C}* \\ \dfrac{-K_1\dfrac{V_o+\tilde{v}_o}{R_L}-LK\left[V_{ref}-\beta(V_o+\tilde{v}_o)\right]+V_i+K_2(I_L+\tilde{i}_L)-K_2K\int\left[V_{ref}-\beta(V_o+\tilde{v}_o)\right]dt}{V_o-K_1\dfrac{V_o^2}{V_iR_L}}-\dfrac{V_o+\tilde{v}_o}{R_LC} \end{cases} \quad (26)$$

V_o and I_L are fixed values and their derivatives are equal to zero, and (27) is obtained by solving (26).

$$\begin{cases} \dfrac{d\tilde{i}_L}{dt}=a_{11}\tilde{i}_L+a_{12}\tilde{v}_o+a_{13}\int\tilde{v}_o dt \\ \dfrac{d\tilde{v}_o}{dt}=a_{21}\tilde{i}_L+a_{22}\tilde{v}_o+a_{23}\int\tilde{v}_o dt \\ \dfrac{d\int\tilde{v}_o dt}{dt}=a_{31}\tilde{i}_L+a_{32}\tilde{v}_o+a_{33}\int\tilde{v}_o dt \end{cases} \quad (27)$$

$$a_{11}=\frac{K_2V_iR_L}{L(K_1V_o-V_iR_L)};a_{12}=\frac{LK\beta V_iR_L-2K_1V_i+K_2V_o}{L(K_1V_o-V_iR_L)};a_{13}=\frac{K_2K\beta V_iR_L}{L(K_1V_o-V_iR_L)}$$

$$a_{21}=\frac{2K_2V_o-K_1V_i}{C(K_1V_o-V_iR_L)};a_{22}=\frac{-LK\beta V_o+V_i}{C(K_1V_o-V_iR_L)};a_{23}=\frac{-K_2K\beta V_o}{C(K_1V_o-V_iR_L)}$$

$$a_{31}=a_{33}=0;a_{32}=1$$

Equation (27) is the linear system equation around the equilibrium point that is transformed in the form of standard state equations as follows:

$$Determinant\,[\mathrm{SI}-\mathrm{A}]=0 \quad (28)$$

where I and A are the 3x3 identity matrix and the coefficients matrix, respectively.

$$\mathrm{SI}-\mathrm{A}=\begin{pmatrix} S-a_{11} & -a_{12} & -a_{13} \\ -a_{21} & S-a_{22} & -a_{23} \\ 0 & -1 & S \end{pmatrix} \quad (29)$$

where a_{ij} is obtained as follows:

$$S(S-a_{11})(S-a_{22})-a_{13}a_{21}-a_{23}(S-a_{11})-a_{12}a_{21}S=0$$

$$S^3+P_1S^2+P_2S+P_3=0$$

$$P_1=-a_{11}-a_{22};P_2=a_{11}a_{22}-a_{12}a_{21}-a_{23};P_3=a_{11}a_{23}-a_{13}a_{21}$$

$$P_1\geq 0;P_2\geq\frac{P_3}{P_1};P_3\geq 0 \quad (30)$$

Conditions (30) must be satisfied. By applying the conditions specified in these relations, the range for the unknown coefficients K_1 and K_2 will be obtained as long as the poles remain on the left side of the imaginary axis. For having the maximum range of variations for R_L and V_i, the mean points of coefficients K_1 and K_2 are considered. The proposed control circuit is shown in Fig. 5.

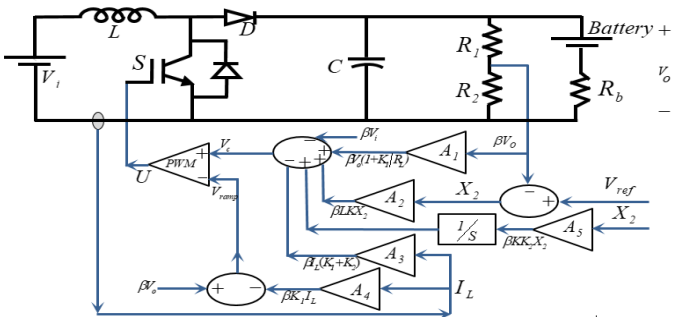


Fig. 5. A schematic diagram of the proposed integral sliding mode control to be used in EVBC

V. Simulation Results

Simulations were performed in Matlab Simulink at three SOC levels of 20%, 50%, and 80% to have a comprehensive survey of the proposed controller's performance

Table1. The parameter values used in the simulation

Parameters		Quantities	Parameters	Quantities
Vo		400 V	L	2 mH
Vi	0 s < t < 3.5 s	160 V	K	100
	3.5 s < t < 7 s	170 V	K1	2.5
	t > 7 s	160 V	K2	35
Fs		50 kHZ	Simulation duration	7 sec (0 -7)
β		1	SOC	%20,%50,%80
C		680 μF	RL	0.5 Ω

Tables 1 and II and Fig. 6 present all parameters' quantities and battery charging current/voltage parameters in an example for more clearness, respectively. Moreover, all parameters of battery charging voltage such as Error, Ripple, %Ripple, and %Mean Displacement are distinctly considered in all SOCs in Figs. 7(a), 7(c), and 7(e). Similarly, Ripple and %Ripple of battery charging current in all SOCs are distinctly considered as well in Figs. 7(b), 7(d), and 7(f). The proposed controller demonstrates how well it controls those parameters in comparison with the other SMCs in all mentioned Figures.

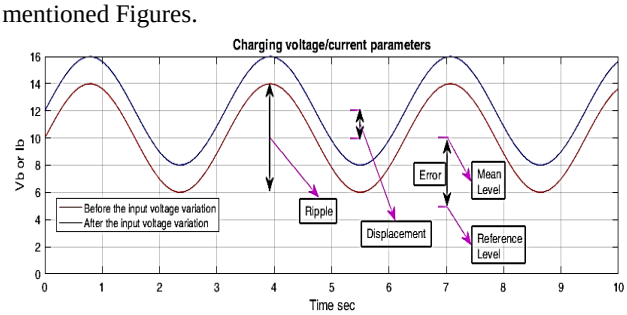
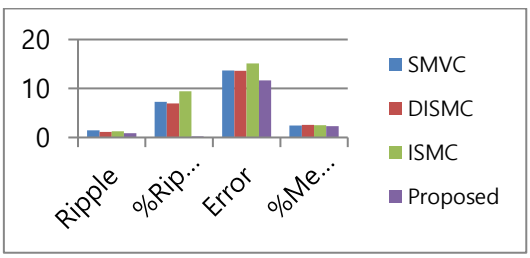


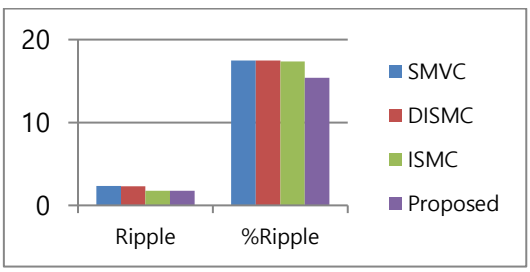
Fig. 6. The presentation of battery charging current/voltage parameters in an example diagram for more clearness

Table II. The definitions of the voltage/current parameters

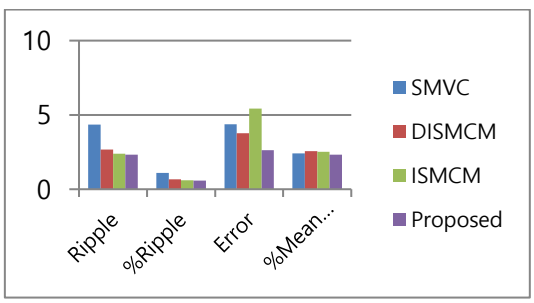
Parameters	Explanations	Equations
%Mean Displacement	The output displacement directly affected by input variation	$\%Mean.Displacement = \frac{Displacement}{V_{before.input.variation}(I_{before.input.variation}) + Displacement/2} x\,100$
Error	Difference between the output and its reference	$Error = V_{o\cdot Mean}(I_{o\cdot Mean}) - V_{ref}(I_{ref})$
Ripple	The output peak to peak	$Ripple = V_{peak^+}(I_{peak^+}) - V_{peak^-}(I_{peak^-})$
%Ripple	Multiplying the output peak to peak divide by its mean by 100	$\%Ripple = 100 \cdot \frac{V_{peak^+}(I_{peak^+}) - V_{peak^-}(I_{peak^-})}{V_{mean}(I_{mean})}$



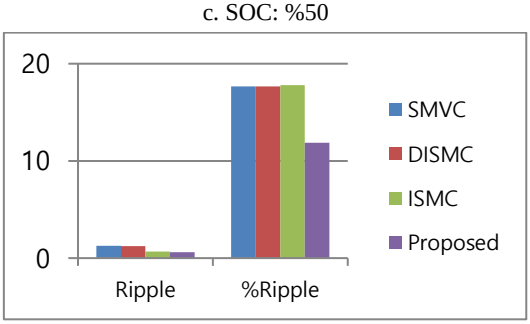
a. SOC: %20



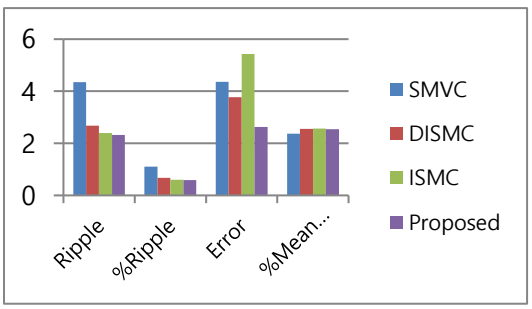
b. SOC: %20



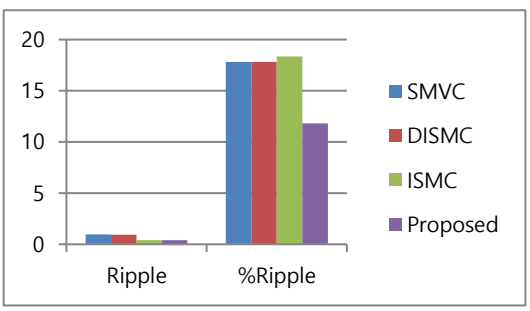
c. SOC: %50



d. SOC: %50



e. SOC: %80



f. SOC: %80

Fig.7. The proposed controller charging voltage and current parameters in comparison with the other SMCs.

Fig. 8 depicts the charging battery voltage for the proposed controller compared to the other SMCs on the three SOCs specified in Table I. According to all parts of Fig. 8, the battery charging voltage is close to its reference on SOC 80%. Therefore, the voltage error of its reference lessens by an increase in SOC's amount. Moreover, this parameter in the proposed controller has the lowest amount in comparison with the other SMCs.

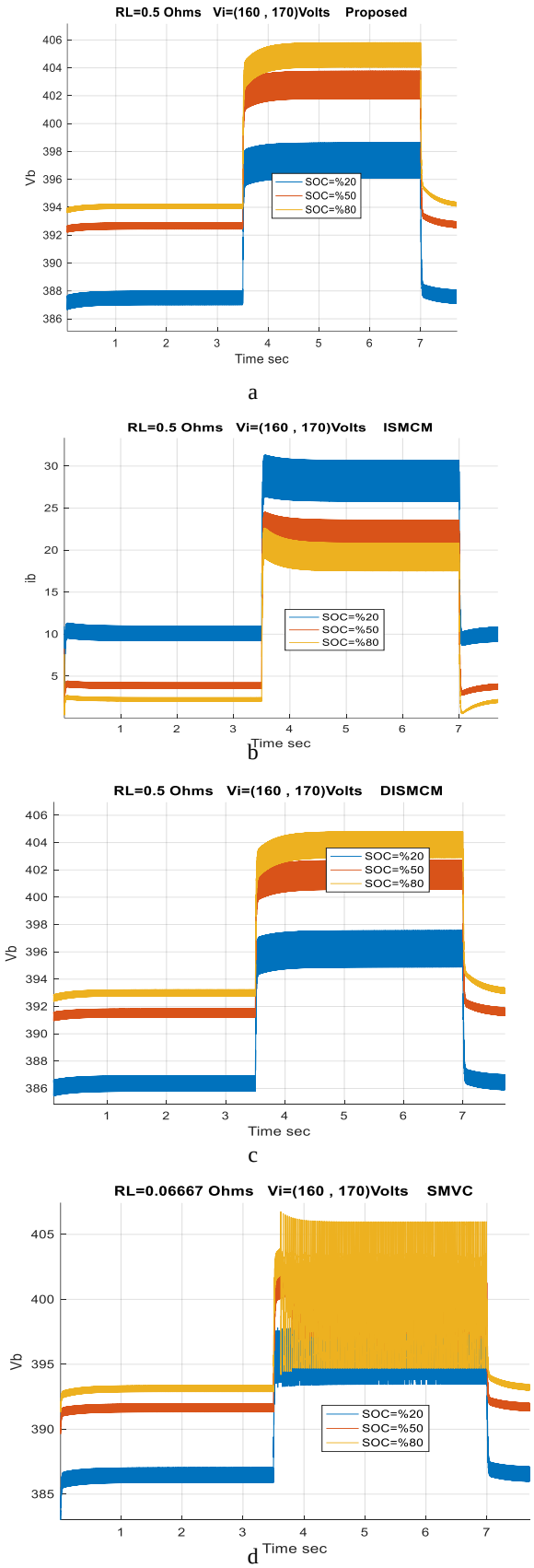
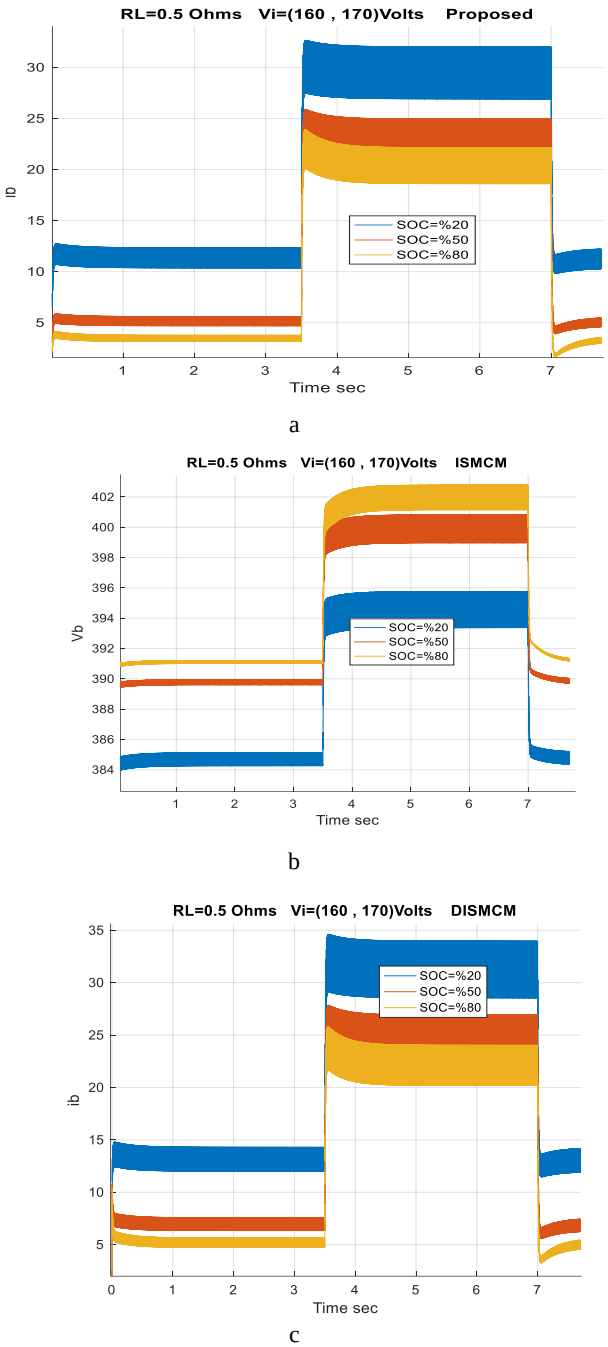
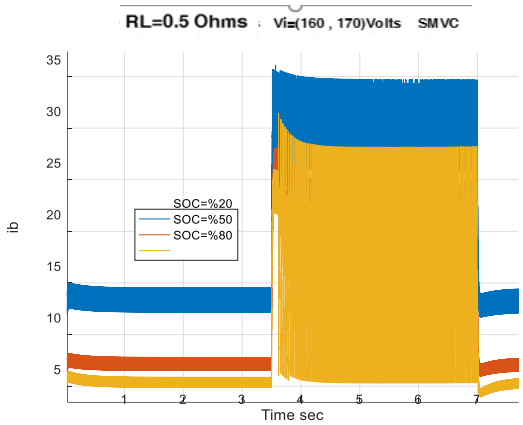


Fig.8. Battery charging voltage-time characteristics for the proposed controller and the other SMCs.

Fig. 9 depicts the charging battery current for the proposed controller compared to the other SMCs on the three SOCs specified in Table I. An extensive charging current ripple is clearly seen by input variations in Fig. 9(d).





d

Fig.9. Battery charging current time characteristics for the proposed controller and the other SMCs.

VI. CONCLUSIONS

An improved SMC applicable in a DC/DC boost converter as an EVBC is presented in this paper. Based on the simulation results, all charging voltage and input current parameters demonstrate how the proposed controller keeps those to a minimum based on the comparisons with the other SMCs. Ripple, error, mean displacement, and their percentages were considered as the parameters mentioned above. A more robust structure in the input power supply voltage variations is another distinctive characteristic of the proposed controller. This property is attained by making a comparison between the input current and integral function of the charging voltage error parameter. Moreover, this allows flexibility in the input voltage level variations. Therefore, this controller makes it possible to use various kinds of input power supplies such as RESs, PVCs, wind turbines, and ancillary batteries for EVBCs.

REFERENCES

[1] A.V. J. S. Praneeth, and Sh. S Williamson, "A Review of Front End AC-DC Topologies in Universal Battery Charger for Electric Transportation," *2018 IEEE Transportation Electrification Conference and Expo (ITEC)*, DOI: 10.1109/ITEC.2018.845018630, August 2018.

[2] M. Y. Metwly, M. S. Abdel-Majeed, A. S. Abdel-Khalik, R .A Hamedy, and M. S. Hamad, "A Review of Integrated On-Board EV Battery Chargers Advanced Topologies Recent Developments and Optimal Selection of FSCW Slot Pole Combination," *IEEE Access*, pp. 85216 – 8524206, DOI: 10.1109/ACCESS.2020.2992741, May 2020.

[3] S. Kumar, and A. Usman, "A Review of Converter Topologies for Battery Charging Applications in Plug-in Hybrid Electric Vehicles," *2018 IEEE Industry Application Society Annual Meeting (IAS)*, DOI: 10.1109/IAS.2018.8544609, 29 November 2018.

[4] A. Taheri, and N. Asghari, "Sliding Mode Control of LLC Resonant DC-DC Converter for Wide output voltage Range in Battery Charging Applications," *2019 International Journal of Industrial Electronics (IECO)*, pp. 127-136, DOI: 10.22111/IECO.2018.27333.1096, April 2019.

[5] M. R. Shokoohinia, and M. M. Fateh, "Model-free tracking control via adaptive dynamic sliding mode control with application to robotic systems," *2020 International Journal of Industrial Electronics (IECO)*, DOI: 10.22111/ieco.2020. 31596.1207, 2020.

[6] J. Keighobadi, and M. M. Fateh, "Adaptive Robust Tracking Control Based on Back stepping Method for Uncertain Robotic Manipulators Including Motor Dynamics," *2020 International Journal of Industrial Electronics (IECO)*, DOI: 10.22111/ ieco.2020.31792.1213, 2020.

[7] A. Noori, M. A. Sadrnia, and M. B. Naghibi-Sistani, "Fault Tolerant Control of Blood Glucose Concentration Using Reinforcement Learning," *2020 International Journal of Industrial Electronics (IECO)*, pp. 353-364 DOI: 10.22111/ ieco.2020.31719.1217, July 2020.

[8] A. Tiwari, O. Jaga, and Sh. Singh Soni, "Sliding mode controller based interleaved boost converter for fuel cell," *2017 Recent Developments in Control, Automation & Power Engineering (RDCAPE)*, DOI: 10.1109/RDCAPE. 2017. 8358325, 14 May 2018.

[9] F. Z. Belhaj, H. El Fadil, A. Tahri, K. Gaouzi, A. Rachid, and F. Giri "Sliding mode control of cascade boost converter for fuel cell energy generation system," *2017 International Conference on Electrical and Information Technologies (ICEIT)*, DOI: 10.1109/EITech.2017.8255239, 15 January 2018.

[10] V. M. Iyer, S. Gulur, and S. Bhattacharya, "Variable dc bus control for a bidirectional on-board EV charger," *2017 IEEE 6th International Conference on Renewable Energy Research and Applications (ICRERA)*, DOI: 10.1109/ICRERA.2017. 8191216, 14 December 2017.

[11] D. Patil, and V. Agarwal, "Compact on-board single-phase EV battery charger with novel low frequency ripple compensator and optimum filter design," *IEEE Transactions on Vehicular Technology*, Vol. 65, No. 4, DOI: 10.1109 / TVT. 2015. 2424927, 21 April 2015.

[12] A. Karaarslan, "The analysis of average sliding control method applied on Sheppard-Taylor power factor correction converter," *Electronics Engineering (2013)* 95:255–265 DOI 10.1007/s00202-012-0257-3, 23 September 2012.

[13] A. Mallik, J. Lu, and A. Khaligh, "Sliding mode control of single phase interleaved totem-pole PFC for electric vehicle on-board chargers," *2018 IEEE Transactions on Vehicular Technology*, Vol. 67, No. 9, pp. 8100-8109, DOI: 10. 1109/ TVT.2018.2848238, 18 June 2018.

[14] P. Guerriero, M. Coppola, D. Lauria, and S. Daliento, " PWM Based Sliding Mode Control of a fast charger for super capacitors," *2020 International Symposium on Power Electronics, Electrical Drives, Automation and Motion (SPEEDAM)*, DOI**:** 10.1109/SPEEDAM48782.2020.9161872, 7 August 2020.

[15] A. Verma, B. Singh, A. Chandra, and K. Al-Haddad, "An Implementation of Solar PV Array Based Multifunctional EV Charger," *2018 IEEE Transportation Electrification Conference and Expo (ITEC)*, DOI**:** 10.1109 / ITEC. 2018. 8450191, 30 August 2018.

[16] J. Ackermann, and V. Utkin, "Sliding mode control design based on Ackermann's formula," *IEEE Transactions on Automatic Control* Vol. 43, No. 2, pp. 234–237, DOI: 10.1109/9.661072, , Feb 1998.

[17] R. Redl, N. O. Sokal, "Current-mode control, five different types, used with the three basic classes of power converter: Small-signal AC and large-signal DC characterization, stability requirements, and implementation of practical

circuits," *1985 IEEE Power Electronics Specialists Conference*, DOI: 10.1109/PESC.1985.7071020, 30 March 2015.

[18] Siew-Chong Tan&Yuk-Ming Lai&Chi Kong Tse, "Sliding Mode Control of Switching Power Converters-Techniques and Implementation," *Boca Raton, FL 33487-2742© 2012 by Taylor & Francis Group*, 2012.



Gholamreza Mohebalizadeh was born in Tehran, Iran, in 1967. He received a B.Sc. degree in electronic engineering from the University of Shiraz, Shiraz, in 1991, an M.Sc. degree in nuclear engineering from Tehran Azad University, Tehran, Iran, in 2000, and he is a Ph.D. candidate in electrical engineering from Islamic Azad University, Shabestar Branch. His current research interests include power electronic converters and renewable energy systems.



Hasan Alipour received his B.Sc., M.Sc., and Ph.D. degrees in power electrical engineering from Iran University of Science and Technology (IUST), Tehran, Iran, in 2008, the University of Tehran, Tehran, Iran, in 2011, and the University of Tabriz, Tabriz, Iran, in 2015, respectively. Currently, he is an assistant professor in the engineering faculty of Islamic Azad University, Shabestar Branch. His research interest focuses on electric and hybrid electric vehicles, electric machines drive, linear electric motors, renewable energies, and distributed generation.



Leila Mohammadian was born in Tabriz, Iran in 1984. She received her B.Sc., M.Sc., and Ph.D. degrees in Electrical Engineering from the Department of Electrical and Computer Engineering, University of Tabriz, Tabriz, Iran, in 2007, 2011, and 2015, respectively. She has been with Shabestar Branch, Islamic Azad University, Shabestar, Iran since 2011. She has been an assistant professor since 2015. Her current research interests include the analysis and control of power electronic converters and their applications.



Mehran Sabahi was born in Tabriz, Iran, in 1968. He received his B.Sc. degree in electronic engineering from the University of Tabriz, Tabriz, in 1991, his M.Sc. degree in electrical engineering from Tehran University, Tehran, Iran, in 1994, and his Ph.D. degree in electrical engineering from the University of Tabriz, in 2009. In 2009, he joined the Faculty of Electrical and Computer Engineering, University of Tabriz, where he has been an associate professor since 2014. His current research interests include power electronic converters and renewable energy systems.